# LES of an auto-igniting $C_2H_4$ flame DNS

**By E. Knudsen, E. S. Richardson, J. H. Chen AND H. Pitsch**

## 1. Motivation and objectives

Large eddy simulation (LES) combustion modeling capabilities have been steadily improving for some time. Nonetheless, many classes of turbulent reactive flows remain difficult to describe using LES. These difficulties arise because combustion is characterized by highly non-linear, mixing-dependent physics that often occur on subfilter LES scales. Some of the newest tools that are being used to address these difficulties are the peta-scale direct numerical simulations (DNS) of flames now being generated at national laboratories (Sankaran *et al.* 2007; Yoo *et al.* 2011). Advancing computational infrastructure has enabled the operation of these simulations at Reynolds numbers that are commonly associated with laboratory validation flames (Barlow *et al.* 2005; Cabra *et al.* 2005). Additionally, complex chemical mechanisms that are non-linearly sensitive to realistic transport and turbulence effects are used in each DNS. The cases therefore serve as an excellent platform for LES combustion model validation. Examples of such validation studies include the CMC analysis of Richardson *et al.* (2009) and the LES scalar dissipation and scalar variance study of Knudsen *et al.* (2011).

Here, several components of a high-fidelity LES combustion model are investigated using an auto-igniting $C_2H_4$ flame DNS from Sandia National Laboratories (Yoo *et al.* 2011). LES studies of the flame are performed using an unsteady flamelet combustion model. Initial simulations demonstrated that the LES/DNS agreement was poor when typical assumptions such as the use of unity Lewis numbers in the flamelet equations were invoked. These results motivated an inquiry into the influence of different components of the unsteady flamelet and LES framework. In the following sections, the results of this inquiry are presented. Three topics in particular are focused upon: 1) accuracy of the unsteady flamelet framework, 2) differential diffusion effects, and 3) sensitivity to LES mesh resolution. It will be demonstrated that the unsteady flamelet model describes the DNS very accurately when turbulent mixing and differential diffusion are accurately accounted for. It will also be confirmed, however, that the modeling framework fails when these processes are misrepresented due to faulty assumptions or poor descriptions of mixing.

The paper is organized as follows. This section serves as an introduction. In section 2, a description of the flame DNS is given. Section 3 introduces the unsteady flamelet combustion model, and section 4 discusses how to identify differential diffusion within an LES flow solver. Section 5 considers the sensitivity of computational LES parameters that are external to the combustion model, but that nonetheless influence agreement with the DNS. LES results are given in section 6, and section 7 summarizes the work.

## 2. Case description

The DNS case that will be used for combustion model validation is an auto-igniting slot jet. This ethylene-fueled flame was originally the subject of a DNS study by Yoo *et al.*

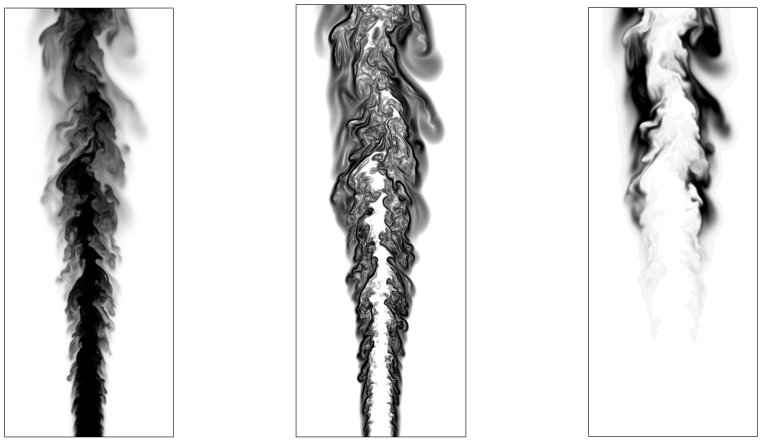

FIGURE 1. Yoo *et al.* (2011)'s lifted flame DNS. Left: Mixture fraction, $Z$, from 0.0 (white) to 1.0 (black). Center: Mixture fraction dissipation rate, $\chi_Z$, on a log scale from 1.0 $s^{-1}$ (white) to 6000 $s^{-1}$ (black); Right: Progress variable, $C$, from 0.0 (white) to 0.2 (black).

(2011). A schematic of the flame appears in Figure 1, where mixture fraction ($Z$), scalar dissipation rate ($\chi_Z$), and progress variable ($C$) contours from the flame are plotted. The central fuel jet has a bulk velocity of 220 m/s, a temperature of 550 K, and a composition of 82% $N_2$ and 18% $C_2H_4$ by volume. The central stream is denoted by a mixture fraction of $Z = 1$. The coflow that surrounds the central jet consists of pure air at a temperature of 1550 K. The coflow enters the domain at a bulk velocity of 20 m/s, and this air stream is denoted by a mixture fraction of $Z = 0$. No nozzle separates the main jet and coflow; rather, the velocity, temperature, and composition profiles are prescribed to smoothly transition between $Z = 0$ and $Z = 1$ according to the functions listed in Yoo *et al.* (2011).

The total width of the central jet is $H = 0.002$ m, and the domain size is $15H \times 20H \times 3H$ in the downstream, cross-stream, and periodic directions, respectively. The jet Reynolds number associated with the DNS conditions is Re=10,000, and the DNS is run at atmospheric pressure. The stoichiometric mixture fraction that results from the use of the diluted ethylene fuel stream is $Z_{st} = 0.27$. The DNS mesh consists of 1.3 billion cells, and the simulation required approximately 14 million CPU hours of run time. Chemistry in the flame is described using a 22 species ethylene mechanism (Yoo *et al.* 2011) that was reduced from a larger hydrocarbon mechanism. This same 22 species mechanism has been used in all of the modeled LES calculations that are shown.

Turbulence is introduced into the jet DNS by extracting velocity information from a single realization of a homogeneous isotropic turbulence (HIT) field, and then superimposing this information on a bulk velocity profile at the inlet of the jet simulation. The turbulence field was synthesized by specifying the length scales and magnitudes of velocity fluctuations, as well as the spectral energy density. As time advances in the reacting jet DNS, the plane from which turbulence data is taken in the HIT field also advances. In all LES calculations shown below, these HIT data are filtered and then injected into the LES as a boundary condition.

## 3. Combustion model

Combustion is modeled using an unsteady flamelet approach similar to that of Pitsch & Ihme (2005) and Ihme & See (2010). The model is implemented by first solving the

unsteady flamelet equations (Peters 2000) for the species $\phi_k$,

$$\rho\frac{\partial(\phi_k)}{\partial\tau} = \frac{1}{\mathrm{Le}_k}\frac{\rho\chi_Z}{2}\frac{\partial^2\phi_k}{\partial Z^2} + \rho\dot{\omega}_k + \frac{1}{4}\left(\frac{1}{\mathrm{Le}_k} - 1\right)\frac{\partial\phi_k}{\partial Z}\left[\frac{\partial(\rho\chi_Z)}{\partial Z} + \frac{\chi_Z}{\mathcal{D}_Z}\frac{\partial(\rho\mathcal{D}_Z)}{\partial Z}\right], \quad (3.1)$$

where $Z$ is the mixture fraction and $\mathrm{Le}_k$ is the Lewis number of the $k^{th}$ species. Note that for brevity this form of the flamelet equations neglects standard molar diffusion correction velocities, even though these velocities are accounted for in the actual flamelet calculations. The initial conditions of the species $\phi_k$ in Eq. (3.1) are linear profiles representing non-reactive mixing between $Z = 0$ and $Z = 1$. The dissipation rate appearing in the equation is modeled as

$$\chi_Z = \chi_{Z,\mathrm{ref}} \cdot \left(f(Z) \,/\, f(Z_{\mathrm{ref}})\right), \quad (3.2)$$

where $f$ is a prescribed function of $Z$ (Peters 2000). Unsteady flamelet solutions are solved using a variety of reference scalar dissipation rates. They are then tabulated as a function of $Z$, $\chi_{Z,ref}$, and the progress variable $C$, which is defined as the sum of four species mass fractions,

$$C = Y_{H_2O} + Y_{H_2} + Y_{CO} + Y_{CO_2}. \quad (3.3)$$

This progress variable behaves as a time-like coordinate in flamelet space. The specification of each species' Lewis number is discussed in detail in section 4, but the mixture fraction and progress variables are assumed to have Lewis numbers of unity.

Once generated, the unsteady solutions are convoluted with presumed PDFs for application in the LES. A beta PDF is presumed to describe $Z$, while a delta PDF is presumed to describe $\chi_{Z,ref}$. Additionally, it is assumed that a single unsteady flamelet solution is representative of the conditions in an LES mesh cell. Consequently, only the mean value of the progress variable is needed for modeling (Pierce & Moin 2004). These assumptions lead to a tabulated LES chemistry database of the form

$$\widetilde{\phi}_k = \widetilde{\phi}_k(\widetilde{Z}, \widetilde{Z''^2}, \chi_{Z,\mathrm{ref}}, \widetilde{C}), \quad (3.4)$$

where $\phi_k$ is any reacting quantity of interest. The reference dissipation rate can be determined from the local unconditional LES dissipation rate $\overline{\chi}_Z$ by filtering Eq. (3.2),

$$\chi_{Z,\mathrm{ref}} = \overline{\chi}_Z \cdot \left(f(Z_{\mathrm{ref}}) \,/\, \overline{f(Z)}\right), \quad (3.5)$$

where $\overline{f(Z)}$ is determined by convoluting the function $f(Z)$ with a beta PDF.

## 4. Evaluating differential diffusion effects in LES

Differential diffusion describes the tendency of chemical species to molecularly diffuse at different rates. Each species' molecular diffusivity is denoted by its Lewis number, and so-called Lewis number effects are present to a greater or lesser degree in every physical flame. For example, differential diffusion has often been experimentally isolated in turbulent flames (Smith *et al.* 1995; Bergmann *et al.* 1998; Drake *et al.* 1981), even though it is typically associated with more laminar flow conditions. In an analysis of Lewis number effects, Pitsch (2000) noted three possible conditions under which differential diffusion must be accounted for in turbulent combustion: 1) a laminarized flow field near a jet nozzle; 2) the local turbulent diffusivity $\mathcal{D}_t$ remaining small relative to the local molecular diffusivity $\mathcal{D}_Z$, and 3) the thickness of a mixture fraction mixing layer near a nozzle being

small relative to the Kolmogorov scale. In the $C_2H_4$ flame being considered here, conditions 1) and 3) are not germane because turbulence with a Kolmogorov scale smaller than the mixing width is injected at the domain inlet. Condition 2) is more relevant, and it can be considered, according to Pitsch's suggestion, by comparing the turbulent diffusivity and the molecular diffusivity of the mixture fraction. This is consistent with other work noting that the importance of differential diffusion scales with the inverse of the Reynolds number (Smith *et al.* 1995). Similarly, Peters (2000) forms an effective Lewis number for a species $k$ using the turbulent diffusivity.

In this section Pitsch's and Peters' suggestions are considered in an effort to understand turbulence's role in diminishing Lewis number effects, and to elucidate the coefficients that should also appear in the ratio of turbulent and molecular diffusivites. This extension is motivated by the observation that it would be beneficial to have access to an LES tool that quantitatively characterizes the importance of Lewis numbers at an arbitrary flow field location, and for an arbitrary fuel. It will be confirmed that the ratio of turbulent and molecular diffusivities plays a role in such a tool, but it will also be argued that this diffusivity alone is an insufficient description of the relevant physics.

### 4.1. *A filtered flamelet transformation*

The flamelet equations are often derived by transforming a scalar transport equation's coordinate basis from physical space into mixture fraction space. The effects of differential diffusion in LES can be quantified by performing a similar coordinate transformation on a filtered equation. The starting point of this transformation is the LES filtered equation for the $k^{th}$ chemical species. After a turbulent diffusivity model for the subfilter flux is introduced into this equation, it reads

$$\frac{\partial}{\partial t}(\overline{\rho}\widetilde{\phi}_k) + \frac{\partial}{\partial x_j}(\overline{\rho}\widetilde{u}_j\widetilde{\phi}_k) = \frac{\partial}{\partial x_j}\left(\overline{\rho}(\mathcal{D}_k + \mathcal{D}_t)\frac{\partial}{\partial x_j}(\widetilde{\phi}_k)\right) + \overline{\rho}\widetilde{\dot{\omega}}_k, \tag{4.1}$$

where $\mathcal{D}_k$ is the molecular diffusivity and $\mathcal{D}_t$ is the turbulent diffusivity. The transformation rules that change this equation's coordinate basis from physical space into filtered mixture fraction space are

$$\frac{\partial}{\partial x_j}(\cdot) \rightarrow \frac{\partial \widetilde{Z}}{\partial x_j}\frac{\partial}{\partial \widetilde{Z}}(\cdot) + \epsilon; \qquad \frac{\partial}{\partial t}(\cdot) \rightarrow \frac{\partial \widetilde{Z}}{\partial t}\frac{\partial}{\partial \widetilde{Z}}(\cdot) + \frac{\partial}{\partial \tau}(\cdot) + \epsilon, \tag{4.2}$$

where $\epsilon$ describes changes along coordinates other than $\widetilde{Z}$. Application of these rules to the filtered $\widetilde{\phi}_k$ equation produces a filtered unsteady flamelet equation and a series of terms that scale with $\epsilon$,

$$\begin{aligned}\overline{\rho}\ \frac{\partial(\widetilde{\phi}_k)}{\partial t} &= \mathcal{O}(\epsilon) + \overline{\rho}\widetilde{\dot{\omega}}_k + \frac{\overline{\rho}\widetilde{\chi}_T}{2}\frac{\partial^2(\widetilde{\phi}_k)}{\partial \widetilde{Z}^2} \\ &+ \frac{\overline{\rho}\widetilde{\chi}_M}{2}\frac{\partial^2(\widetilde{\phi}_k)}{\partial \widetilde{Z}^2} + \left(\frac{1}{\mathrm{Le}_k} - 1\right)\left[\frac{\overline{\rho}\widetilde{\chi}_M}{2}\frac{\partial^2(\widetilde{\phi}_k)}{\partial \widetilde{Z}^2} + \frac{1}{4}\left(\frac{\partial(\widetilde{\phi}_k)}{\partial \widetilde{Z}}\frac{\partial(\overline{\rho}\widetilde{\chi}_M)}{\partial \widetilde{Z}} + \frac{\widetilde{\chi}_M}{\mathcal{D}_Z}\frac{\partial(\rho\mathcal{D}_Z)}{\partial Z}\right)\right].\end{aligned} \tag{4.3}$$

Terms scaling with $\epsilon$ are expected to be more important than the higher-order terms that typically appear in the unfiltered flamelet equations, since the subfilter scalar variance may fluctuate along isosurfaces of $\widetilde{Z}$. Nonetheless, it will be assumed that $\widetilde{\phi}_k$ is primarily a function of $\widetilde{Z}$, $\tau$, and the dissipation rate, so that all $\epsilon$ terms can be neglected. Mixing terms associated with one dissipation rate, $\widetilde{\chi}_T$, appear on the first line of Eq. (4.3), while mixing terms associated with a different dissipation rate, $\widetilde{\chi}_M$, appear on the second line.

These two dissipation rates are defined as

$$\widetilde{\chi}_T = 2\mathcal{D}_t|\nabla\widetilde{Z}|^2, \qquad \widetilde{\chi}_M = 2\mathcal{D}_Z|\nabla\widetilde{Z}|^2, \tag{4.4}$$

where the $T$ and $M$ subscripts denote the fact that $\mathcal{D}_t$ is a turbulent diffusivity and $\mathcal{D}_Z$ is a molecular diffusivity. The $Z$ subscript indicates that the molecular diffusivity of the mixture fraction is being considered.

In Eq. (4.3) all non-unity Lewis number effects appear in the second line, and induce mixing at a rate of $\widetilde{\chi}_M$. No Lewis numbers appear in terms containing $\widetilde{\chi}_T$ because the turbulent diffusivity that models the subfilter transport of $\widetilde{Z}$ is assumed to be the same turbulent diffusivity that models the transport of $\widetilde{\phi}_k$. From a physical perspective, the subfilter transport of both $\widetilde{Z}$ and $\widetilde{\phi}_k$ is modeled using the single diffusivity $\mathcal{D}_t$ because this transport is caused by the same velocity field. Convective transport treats these variables the same and is not a function of Lewis number. In LES, subfilter convection is modeled using a turbulent diffusivity, and the $\widetilde{\chi}_T$ mixing term in Eq. (4.3) is simply an explicit representation of this subfilter convection.

Equation (4.3) is a quantitative realization of how differential diffusion diminishes in importance as the Reynolds number (Re) increases. $\mathcal{D}_k$ is independent of Re, while $\mathcal{D}_t$ generally increases as the LES filter width is held constant and Re grows larger. Consequently, in high-turbulence environments $\widetilde{\chi}_T$ is large relative to $\widetilde{\chi}_M$, and all $\widetilde{\chi}_M$ terms, including the non-unity Lewis number terms, can be treated as small. As discussed in further detail below, however, this analysis does not tell the complete story of turbulence and differential diffusion interaction.

### 4.2. *Modeling differential diffusion's influence*

One method of quantifying the local influence of differential diffusion in an LES is to calculate the ratio of differential diffusion transport to total diffusive transport. From Eq. (4.3), the differential diffusion transport term of species $k$ is to leading order

$$\left(\frac{1}{\mathrm{Le}_k} - 1\right)\frac{\overline{\rho}\widetilde{\chi}_M}{2}\frac{\partial^2(\widetilde{\phi}_k)}{\partial\widetilde{Z}^2}, \tag{4.5}$$

while the total transport term, consisting of contributions from both turbulent transport and unity Lewis number molecular transport, is

$$\frac{\overline{\rho}(\widetilde{\chi}_T + \widetilde{\chi}_M)}{2}\frac{\partial^2(\widetilde{\phi}_k)}{\partial\widetilde{Z}^2}. \tag{4.6}$$

The ratio of these two transport processes is

$$\Theta_{k,\mathrm{Le}} = \frac{\widetilde{\chi}_M\left(\frac{1}{\mathrm{Le}_k} - 1\right)}{\widetilde{\chi}_M + \widetilde{\chi}_T} = \frac{\mathcal{D}_Z\left(\frac{1}{\mathrm{Le}_k} - 1\right)}{\mathcal{D}_Z + \mathcal{D}_t}. \tag{4.7}$$

This ratio is in agreement with the ratio suggested by Pitsch (2000), with $\Theta_{k,\mathrm{Le}}$ rescaled to account for the Lewis number of a particular species.

### 4.3. *Differential diffusion, LES resolution, and the flamelet approximation*

While representative of a particular type of turbulence and diffusion interaction, the transport comparison in Eq. (4.7) does not exhaustively describe the conditions under which differential diffusion effects can be negated. For example, flame structures consistent with unity Lewis numbers can be found in experiments where no LES filter is applied. Because of this lack of filtering, the turbulent diffusivity $\mathcal{D}_t$ is identically zero and the

indicator in Eq. (4.9) would incorrectly suggest the use of non-unity Lewis numbers. To account for these physics, further possibilities must be considered.

Such a discussion begins with the realization that the dissipation rate alone cannot be used to explain the appearance of unity Lewis flame structures, since fully resolved non-unity Lewis number mixing terms scale with the same $\chi_Z$ parameter that unity Lewis number mixing terms scale with. An increase in turbulence that leads to an increase in $\chi_Z$ therefore fails to explain changes in differential diffusion's influence under fully resolved conditions.

An alternative explanation for the presence of unity Lewis number flame structures under fully resolved conditions is that the flamelet approximation breaks down. If transport occurs along directions other than those aligned with the $Z$ coordinate, then the formalism of Eq. (3.1) breaks down, and a pathway appears for arguing that non-unity Lewis number terms can be neglected. For example, accounting for a direction that is orthogonal to $Z$ in the flamelet equation derivation leads to the appearance of a convection term on the right-hand side of Eq. (3.1) of the form

$$-\rho u_\epsilon \frac{\partial \phi_k}{\partial \epsilon}, \tag{4.8}$$

where the $\epsilon$ coordinate is aligned with a direction orthogonal to the local gradient of $Z$, and where $u_\epsilon$ is the flow velocity in that direction. The $\partial\phi_k/\partial\epsilon$ derivative is normally treated as negligibly small in non-premixed flames. If turbulence is intense and this gradient increases, or if molecular diffusion is slow relative to convective mixing, the term will account for turbulent mixing between flamelets. Modeling this term's ability to negate Lewis number effects will be the subject of future work. In the remainder of this section the differential diffusion comparison from Eq. (4.7) will be considered with the caveat that while it is computationally useful, it is not fully explanatory.

### 4.4. *Application in the $C_2H_4$ flame*

To determine the importance of Lewis number effects in the $C_2H_4$ flame, the Lewis number transport ratio is time averaged at sequential downstream planes in the jet. The results will be shown below in section 6. The exact quantity that will be calculated is

$$\Theta_{k,\mathrm{Le}} = \left( \frac{\langle \mathcal{D}_Z \rangle}{\langle \mathcal{D}_Z + \mathcal{D}_t \rangle + \epsilon} \right) \left| \frac{1}{\mathrm{Le}_k} - 1 \right|, \tag{4.9}$$

where a small number $\epsilon$ is added to the denominator to ensure realizability, and the absolute value operator is added to mask distinctions between $\mathrm{Le}_k < 1$ transport and $\mathrm{Le}_k > 1$ transport. The $\langle \cdot \rangle$ operator denotes time averaging, which is necessary because the turbulent diffusivity may locally and instantaneously become negative. In coarsely resolved LES where the turbulent diffusivity is large, Eq. (4.9) suggests that molecular transport processes will be negligible and that unity Lewis numbers should be used.

## 5. Computational details

### 5.1. *Transport equations and subfilter modeling*

The LES computations discussed below solve typical low-Mach momentum equations that employ a dynamic Smagorinsky subfilter flux model with Lagrangian averaging (Desjardins 2008; Meneveau *et al.* 1996). An elliptic equation for the pressure is solved at each time step to enforce continuity. The equations for the filtered $C$ and $Z$ scalars that are needed for the combustion model are also solved using dynamic subfilter flux models.

FIGURE 2. Mixture fraction ($Z$) contours, ranging from from 0.0 (white) to 1.0 (black). Left: 1 million cell LES with narrow domain; Center: 1 milion cell LES with wider domain; Right: 23 million cell mesh with narrow domain.

Specification of the subfilter mixture fraction variance and the filtered mixture fraction dissipation rate has been found to be especially important in lifted flames. As demonstrated by Knudsen *et al.* (2011), standard algebraic models for these quantities tend to significantly underpredict the variance and dissipation rates that are observed in the DNS. Improved predictions were observed following the introduction of transport equation models for both $\widetilde{\chi}_Z$ and $\widetilde{Z''^2}$ that employ a novel adapted dynamic closure. These transport equation models will be adopted in the LES computations discussed here. Further details regarding the models can be found in Knudsen *et al.* (2011).

With the quantities $\widetilde{Z}$, $\widetilde{C}$, $\widetilde{Z''^2}$, and $\widetilde{\chi}_Z$ determined from transport equations, the tabulated chemistry database from Eq. (3.4) can be accessed to determine chemical information such as the density and the progress variable source term.

### 5.2. *Computational meshes*

Four LES meshes will be used to assess the influence of boundary conditions and mesh resolution. Two of these meshes consist of 1 million cells, whereas the other two consist of 23 million cells. At each mesh resolution, both a narrow LES domain and a wider LES domain will be considered. The wider domain stretches from Y/H = –10 to Y/H = +10 in the cross-stream direction, and exactly represents the dimensions of the DNS domain. The narrow mesh represents the DNS domain size in the downstream and periodic directions, but the cross-stream domain stretches from Y/H = -6 to Y/H = +6. Contour plots of the filtered mixture fraction field from both 1 million cell LES runs and from the narrow 23 million cell LES run are shown in Figure 2.

The consideration of different LES domain widths is motivated by the Mach number of the central jet in the DNS. While the Mach number of the DNS coflow is negligible, the Mach number of the central jet reaches a peak value of Ma = 0.46. This value remains within a range where a low-Mach flow solver can provide useful predictions, but is large enough that compressibility effects are present. In running the wider domain LES cases that exactly correspond to the DNS domain, a downstream vortex shedding instability was seen to form. This instability can be seen in Figure 2 by comparing the narrow (left plot) and wide (center plot) 1 million cell LES cases. This vortex shedding instability was not observed in the DNS, as seen in the left plot of Figure 1. One possible explanation for this phenomenon is that compressibility effects provide a stabilizing influence on the

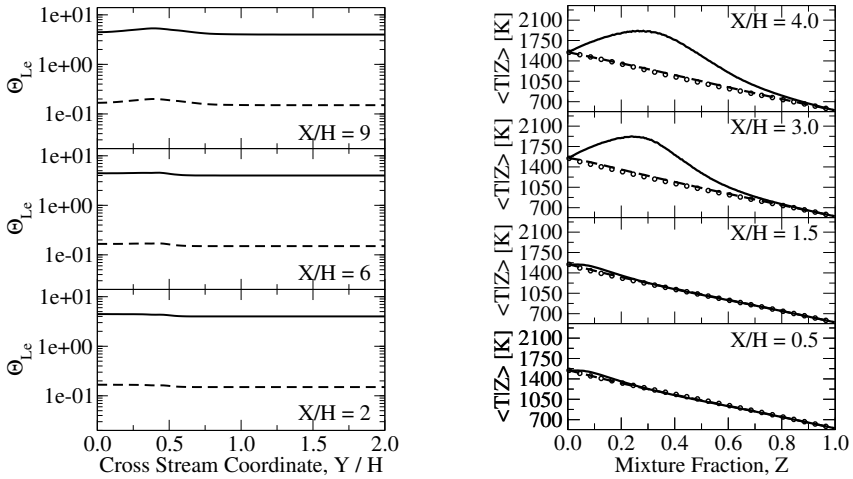


FIGURE 3. Left: Differential diffusion indicator, $\Theta_{\mathrm{Le}}$ from Eq. (4.9), plotted in the 1 million cell LES. Molecular hydrogen with $\mathrm{Le}_{H_2}$=0.2 (——) and ethylene with $\mathrm{Le}_{C_2H_4}$=1.15 (– – –) are shown. Right: Temperature results from experiments (●●), from an LES with unity Lewis number flamelets (——), and from an LES with non-unity Lewis number flamelets (– – –).

DNS. For example, Kennedy & Chen (1998) demonstrate that compressibility effects tend to reduce vorticity formation in slot jets. Interestingly, Kennedy & Chen (1998) also demonstrate that the ratio of the coflow and central jet temperatures is a stronger influence on stability than compressibility effects. In the majority of the $C_2H_4$ flame, the central jet is colder than the ambient gas, which tends to promote stability. The source of the vortex shedding instability therefore warrants further investigation.

Regardless of where the downstream instability originates, it can be eliminated at both LES mesh resolutions by decreasing the width of the LES domain. This effect is seen by comparing the 1 million and 23 million cell meshes in Figure 2. Runs on the narrow LES meshes provide information about the combustion model's performance when downstream mixing is more indicative of the conditions found in the DNS.

## 6. Results and discussion

Figure 3 demonstrates the importance of non-unity Lewis number effects in the flame. The left plot in Figure 3 shows the indicator $\Theta_{k,\mathrm{Le}}$ for both the fuel species $C_2H_4$ (Le = 1.15) and for molecular hydrogen, $H_2$ (Le = 0.2). Throughout the jet, these transport ratios have values of approximately the Lewis number prefactors ($1/\mathrm{Le}_k$ - 1). Nowhere do they approach zero and indicate that subfilter scalar flux dominates molecular transport. Consequently, molecular diffusion processes are important throughout the jet. While the data does not definitively prove that non-unity Lewis number flame structures are present in the case (see discussion in section 4.3), the importance of differential diffusion is confirmed by the right plot in Figure 3. There, LES results from a simulation using unity Lewis number flamelets are compared with LES results from a simulation that uses non-unity Lewis number flamelets. Both simulations are run on the wider 1 million cell mesh, and the modeled dissipation rate $\overline{\chi}_Z$ has been locally rescaled to match the DNS data so that dissipation errors do not influence the results. The simulation that employs unity Lewis number strongly overpredicts chemical source terms, and leads to early ignition. The use of non-unity Lewis numbers, conversely, results in an appropriate

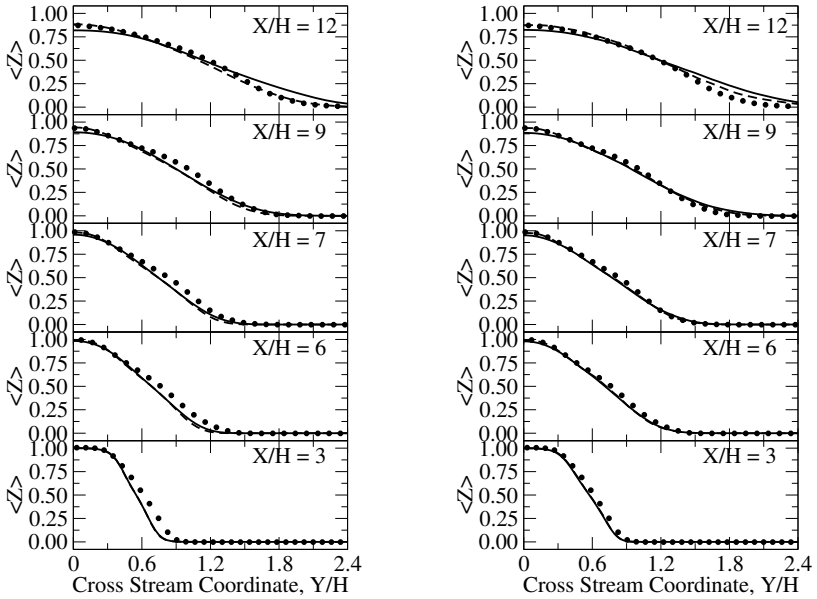


FIGURE 4. Time-averaged $\widetilde{Z}$ profiles in the jet. DNS data (••) are compared with data taken from a wider domain LES (——) and from a narrower domain LES (– – –). The LES meshes consist of 1 million cells (left) and 23 million cells (right).

flame lift-off and better and agreement with the DNS. In the results shown below, all flamelets are solved using constant non-unity Lewis numbers for all chemical species.

Time-averaged mixture fraction profiles from the four LES cases are shown in Figure 4. Agreement between the LES and DNS is generally good, but two important errors can be noted in the LES data. First, the 1 million cell LES runs underpredict the width of the central jet scalar profile at the $X/H = 3$ station. An examination of the 23 million cell LES results on the right side of Figure 4 shows that this error is mesh dependent, and disappears at higher mesh resolutions. The error can be attributed to the LES model's description of turbulent mixing in the shear layer near the inlet. The second error that can be observed in the $\widetilde{Z}$ profiles occurs in the outer shear layer at the $X/H$=12 station. There, both of the LES simulations that use a wider computational domain are seen to overpredict $\widetilde{Z}$. This error is due to the vortex shedding instability that was discussed in section 5. The use of narrower LES domains, which inhibits the formation of these large scale vortices, largely removes the error.

Time-averaged temperature profiles from physical space and from conditional mixture fraction space are shown in Figure 5 and Figure 6, respectively. These plots demonstrate that the unsteady flamelet model performs well when turbulent mixing processes are adequately described. For example, the dashed lines in the rightmost plots of Figure 5 and Figure 6 predict the turbulent ignition process with a high degree of accuracy, and correctly reproduce all DNS temperature data. Conversely, the plots also demonstrate that the combustion model is highly sensitive to descriptions of turbulent mixing. When the $\widetilde{Z}$ profile in the downstream jet shear layer is too diffuse, the temperature is not accurately predicted by the LES. Specifically, the wider domain LES results underpredict the maximum temperature in the Figure 5 $X/H$=12 station, and overpredict temperature near the centerline. More generally, the 1 million cell LES runs tend to have difficulty predicting the ignition process. The conditional temperature plots on the left-hand side

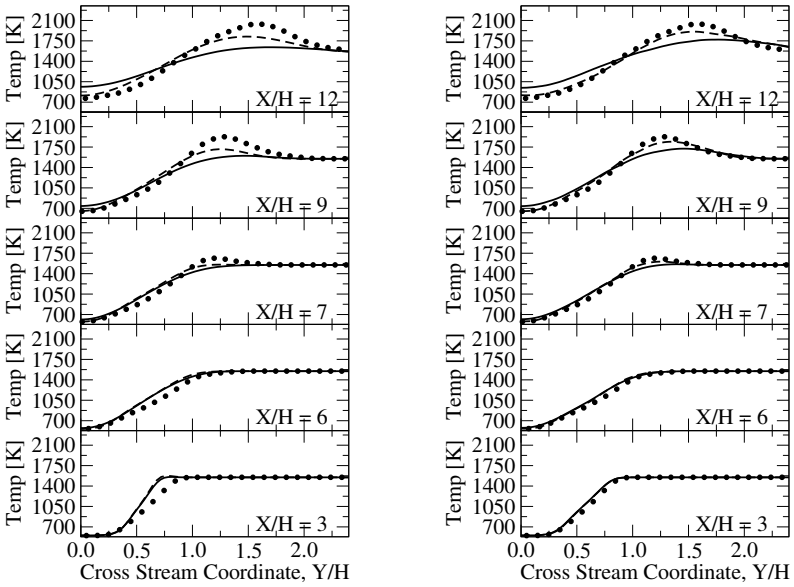


FIGURE 5. Time-averaged temperature in the jet flame. The DNS data (••) are compared with data taken from a wider domain LES (——) and from a narrower domain LES (– – –). The LES meshes consist of either 1 million cells (left) or 23 million cells (right).

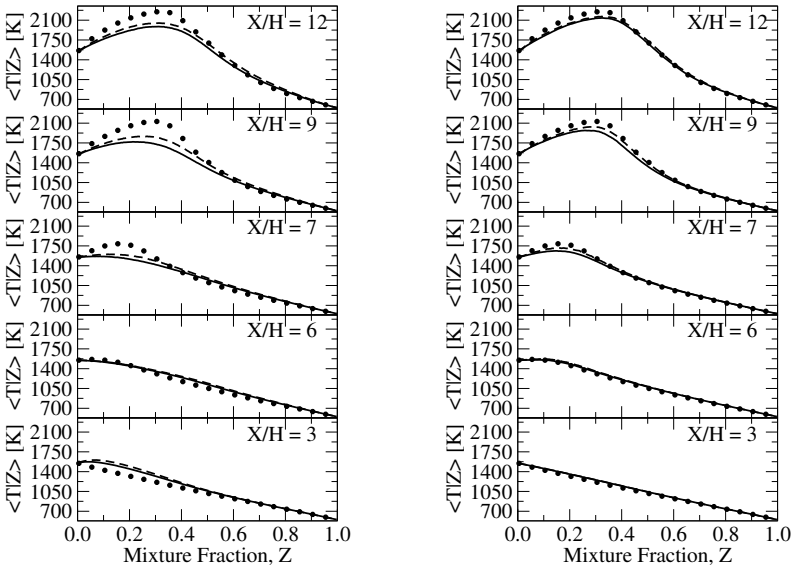


FIGURE 6. Time-averaged conditional temperature in the jet flame. The DNS data (••) are compared with data taken from a wider domain LES (——) and from a narrower domain LES (– – –). The LES meshes consist of either 1 million cells (left) or 23 million cells (right).

of Figure 6 show that the coarse LES ignites too far upstream. The ignition process then slows, however, and the coarse LES underpredicts the DNS conditional temperature profile at downstream locations.

A representative minor species (CO) from the LES runs is plotted in mixture fraction

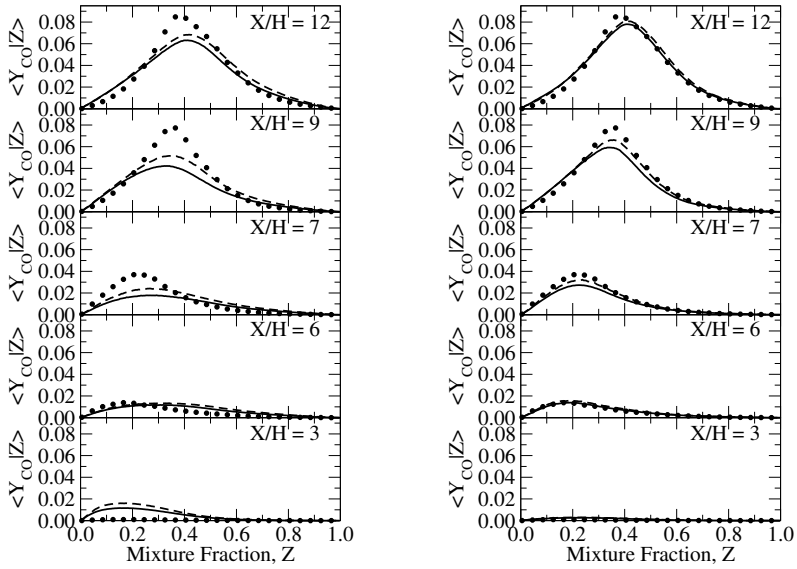


FIGURE 7. Time-averaged CO mass fractions in the jet flame. The DNS data (••) are compared with data taken from a wider domain LES (——) and from a narrower domain LES (– – –). The LES meshes consist of either 1 million cells (left) or 23 million cells (right).

conditioned space in Figure 7. The results confirm the observations that were drawn from temperature data. When turbulent mixing is accurately predicted, the unsteady flamelet model performs well. When the LES mesh resolution decreases, however, agreement with experiments deteriorates. These LES predictions emphasize a continuing need for the study of relationships between mesh cell size, LES filter size, and subfilter mixing models. Specifically, more modeling is needed to address the shortcomings in the predictions of the 1 million cell LES. Although these errors are not caused by the flamelet model itself, the inputs to this model and the model's interaction with the broader LES framework warrant further investigation.

## 7. Summary

A lifted auto-igniting flame DNS has been used to perform LES combustion model validation. The study investigated three issues: 1) the accuracy of an unsteady flamelet combustion model, 2) the importance of differential diffusion effects, and 3) the influence of LES mesh size and boundary conditions. When differential diffusion was appropriately accounted for and turbulent mixing was accurately described, LES simulations indicated that the unsteady flamelet model performed very accurately. The model suffered in accuracy, however, at lower LES resolutions where the jet shear layer was less well resolved. These observations confirm the continuing need for investigations of relationships between mixing models and the reactive LES framework.

## Acknowledgments

Support from the US Air Force Office of Scientific Research (AFOSR), and from the National Aeronautics and Space Administration (NASA) is gratefully acknowledged.

## REFERENCES


Barlow, R. S., Frank, J. H., Karpetis, A. N. & Chen, J.-Y. 2005 Piloted methane/air jet flames: Scalar structure and transport effects. *Combust. Flame* **143**, 433–449.

Bergmann, V., Meier, W., Wolff, D. & Stricker, W. 1998 Application of spontaneous Raman and Rayleigh scattering and 2D LIF for the characterization of a turbulent CH4/H-2/N-2 jet diffusion flame. *Appl. Phys. B* **66** (4), 489–502.

Cabra, R., Chen, J. Y., Dibble, R. W., Karpetis, A. N. & Barlow, R. S. 2005 Lifted methane-air jet flames in a vitiated coflow. *Combust. Flame* **143** (4), 491–506.

Desjardins, O. 2008 Numerical methods for liquid atomization and application in detailed simulations of a diesel jet. PhD thesis, Stanford University.

Drake, M. C., Lapp, M., Penney, C. M., Warshaw, S. & Gerhold, B. W. 1981 Measurements of temperature and concentration fluctuations in turbulent diffusion flames using pulsed Raman spectroscopy. *Proc. Comb. Inst.* **18**, 1521–1531.

Ihme, M. & See, Y. C. 2010 Prediction of autoignition in a lifted methane/air flame using an unsteady flamelet/progress variable model. *Combust. Flame* **157**, 1850–1862.

Kennedy, C. A. & Chen, J. H. 1998 Mean flow effects on the linear stability of compressible planar jets. *Phys. Fluids* **10** (3), 615–626.

Knudsen, E., Richardson, E. S., Doran, E. M., Pitsch, H. & Chen, J. H. 2011 Modeling scalar dissipation and scalar variance in LES: Algebraic and transport equation closures. *Phys. Fluids* (Submitted).

Meneveau, C., Lund, T. S. & Cabot, W. H. 1996 A Lagrangian dynamic subgrid-scale model of turbulence. *J. Fluid Mech.* **319**, 353–385.

Peters, N. 2000 *Turbulent Combustion*. Cambridge, UK: Cambridge Univ. Press.

Pierce, C. D. & Moin, P. 2004 Progress-variable approach for large-eddy simulation of non-premixed turbulent combustion. *J. Fluid Mech.* **504**, 73–97.

Pitsch, H. 2000 Unsteady flamelet modeling of differential diffusion in turbulent jet diffusion flames. *Combust. Flame* **123**, 358–374.

Pitsch, H. & Ihme, M. 2005 An unsteady/flamelet progress variable method for LES of nonpremixed turbulent combustion. $43^{rd}$ *AIAA Aerospace Sciences Meeting, Reno, Nevada* **2005-0557**, 1–14.

Richardson, E. S., Yoo, C. S. & Chen, J. H. 2009 Analysis of second-order conditional moment closure applied to an autoignitive lifted hydrogen jet flame. *Proc. Comb. Inst.* **32**, 1695–1703.

Sankaran, R., Hawkes, E. R., Chen, J. H., Lu, T. & Law, C. K. 2007 Structure of a spatially developing turbulent lean methane-air Bunsen flame. *Proc. Comb. Inst.* **31**, 1291–1298.

Smith, L. L., Dibble, R. W., Talbot, L., Barlow, R. S. & Carter, C. D. 1995 Laser raman scattering measurements of differential molecular diffusion in turbulent nonpremixed jet flames of $H_2$ / $CO_2$ fuel. *Combust. Flame* **100**, 153–160.

Yoo, C. S., Sankaran, R. & Chen, J. H. 2011 A DNS study on the stabilization mechanism of a turbulent lifted ethylene jet flame in highly-heated coflow. *Proc. Comb. Inst.* **33**, 1619–1627.